New Phytologist

Research

Carbon starvation following a decade of experimental drought consumes old reserves in *Pinus edulis*

Drew M. P. Peltier[1], Mariah S. Carbone[1], Cameron D. McIntire[2], Nathan Robertson[3], R. Alex Thompson[4], Shealyn Malone[5], Jim LeMoine[1], Andrew D. Richardson[1,6], Nate G. McDowell[7,8], Henry D. Adams[4], William T. Pockman[3] and Amy M. Trowbridge[5]

[1]Center for Ecosystem Science and Society, Northern Arizona University, Flagstaff, AZ 86011, USA; [2]Northeastern Area State, Private, and Tribal Forestry, USDA Forest Service, 271 Mast Road, Durham, NH 03824, USA; [3]Biology Department, University of New Mexico, Albuquerque, NM 87106, USA; [4]School of the Environment, Washington State University, Pullman, WA 99163, USA; [5]Department of Forest and Wildlife Ecology, University of Wisconsin-Madison, Madison, WI 53706, USA; [6]School of Informatics, Computing, and Cyber Systems, Northern Arizona University, Flagstaff, AZ 86011, USA; [7]Atmospheric Sciences and Global Change Division, Pacific Northwest National Lab, PO Box 999, Richland, WA 99352, USA; [8]School of Biological Sciences, Washington State University, PO Box 644236, Pullman, WA 99164, USA

Author for correspondence:
Drew M. P. Peltier
Email: dmp334@nau.edu

Received: *3 March 2023*
Accepted: *12 June 2023*

New Phytologist (2023)
doi: 10.1111/nph.19119

Key words: bomb-spike, carbohydrates, mortality, nonstructural carbohydrates, radiocarbon, rain-out.

Summary

- Shifts in the age or turnover time of non-structural carbohydrates (NSC) may underlie changes in tree growth under long-term increases in drought stress associated with climate change. But NSC responses to drought are challenging to quantify, due in part to large NSC stores in trees and subsequently long response times of NSC to climate variation.
- We measured NSC age ($\Delta^{14}C$) along with a suite of ecophysiological metrics in *Pinus edulis* trees experiencing either extreme short-term drought (−90% ambient precipitation plot, 2020–2021) or a decade of severe drought (−45% plot, 2010–2021). We tested the hypothesis that carbon starvation – consumption exceeding synthesis and storage – increases the age of sapwood NSC.
- One year of extreme drought had no impact on NSC pool size or age, despite significant reductions in predawn water potential, photosynthetic rates/capacity, and twig and needle growth. By contrast, long-term drought halved the age of the sapwood NSC pool, coupled with reductions in sapwood starch concentrations (−75%), basal area increment (−39%), and bole respiration rates (−28%).
- Our results suggest carbon starvation takes time, as tree carbon reserves appear resilient to extreme disturbance in the short term. However, after a decade of drought, trees apparently consumed old stored NSC to support metabolism.

Introduction

Forests are fundamental components of the global carbon cycle (Bonan, 2008) and experiencing more frequent drought stress (Williams *et al.*, 2020, Zhang *et al.*, 2020). Predicting future forest carbon dynamics necessitates quantitative understanding of tree physiological processes leading to mortality (Adams *et al.*, 2017). But drought may also lead to physiological impairment such as sustained growth reductions and slow postdrought recovery (Anderegg *et al.*, 2015; Peltier *et al.*, 2016). That is, even nonlethal perturbations to tree physiological state have major consequences for ecosystem carbon fluxes (Schwalm *et al.*, 2017) and our ability to predict those fluxes (Kolus *et al.*, 2019). More frequent drought, with shorter interdrought recovery times, leads to more severe growth impairment (Peltier & Ogle, 2019; Anderegg *et al.*, 2020). Our understanding of the mechanisms driving such long-term changes in growth under increased drought stress is poor (Kannenberg *et al.*, 2020; Peltier & Ogle, 2020). Structural and physiological changes such as crown dieback or declines in sapwood conducting area may lead to shifts in carbon dynamics (Rood *et al.*, 2000; Trugman *et al.*, 2018). We propose long-term shifts in the cycling and storage of nonstructural carbohydrates (NSC, defined here as sugars and starch) may also limit tree growth under drought.

More frequent drought stress may impact NSC – the physiological intermediate between carbon uptake and metabolism (Dietze *et al.*, 2014) – in multiple ways. Mild-to-moderate drought (i.e. a reduction in precipitation relative to historic means) can directly limit the activity of growth and respiratory processes, sometimes referred to as 'sink limitation' (Fatichi *et al.*, 2014). While strong drought may co-limit carbon sinks and sources (Resco de Dios & Gessler, 2021), such moderate drought may thus lead to transient increases in crown NSC concentrations (particularly sugars, Muller *et al.*, 2011; Peltier *et al.*, 2020). Trees may prioritize NSC storage (including osmoregulation, Hsiao, 1973) over other sinks like growth (Blumstein

et al., 2022), in some cases even during drought stress (Klein *et al.*, 2014; Huang *et al.*, 2021). Drought may also limit the ability to transport NSC (Sevanto *et al.*, 2014). Regulation mechanisms also exist to limit growth in concert with carbon supply over diurnal timescales (Smith & Stitt, 2007).

Yet despite the existence of these prioritization and regulatory processes, observations show that when demand exceeds supply, trees such as *Pinus edulis* ultimately consume starch under drought stress (Anderegg & Anderegg, 2013; Sevanto *et al.*, 2014; Dickman *et al.*, 2015; Wiley *et al.*, 2016; Peltier *et al.*, 2020). Meta-analysis suggests NSC becomes progressively lost when drought becomes severe (Li *et al.*, 2018) or prolonged (He *et al.*, 2020), consistent with the carbon starvation process (McDowell *et al.*, 2022). Following an updated definition in McDowell *et al.* (2022), we define 'carbon starvation' as a process (not an outcome) of shifts in carbon-related metabolism when carbon supply is limited relative to demand, which tend to reduce NSC. Preservation of metabolic functions (respiration, reproduction, and defense) in the absence of climatic conditions favorable to photosynthetic carbon uptake is often described as the primary function of NSC (Chapin III *et al.*, 1990; Kozlowski, 1992; Dietze *et al.*, 2014). If reductions in NSC concentrations under drought are not universal (e.g. Adams *et al.*, 2017), this could be because drought in some cases was not prolonged enough to substantially impact NSC pools, which can be very large (Hoch *et al.*, 2003). Long-duration field drought manipulations in mature trees are essential to evaluate this concept.

Past studies of NSC responses to drought have also been hindered by our inability to differentiate between different sources and ages of NSC, like whether drought impacts new NSC assimilated over the past few days or older NSC accumulated over many years (Carbone *et al.*, 2013). The mean age or turnover time of NSC in plant tissues can be estimated with radiocarbon (^{14}C; Richardson *et al.*, 2013), but this approach has yet to be applied to trees under drought. NSC age could provide unique information on tree carbon balance: for example, in two trees at steady state with identical concentrations of NSC, the tree with an older NSC pool is turning over that NSC at a slower rate and may be less impacted by transient disruptions to carbon uptake. Such changes in pool ages must also be interpreted in concert with changes in pool size. Previous work has shown that canopy starch concentrations often decrease under drought (Dickman *et al.*, 2015; Adams *et al.*, 2017; Li *et al.*, 2018), yet whether this represents a loss of the older stored 'reserve' NSC pool (Richardson *et al.*, 2013) potentially making the tree more vulnerable to future stressors remains unknown. In more mesic systems, the oldest NSC has been found in shade-suppressed trees (Carbone *et al.*, 2013), suggesting loss of young NSC in stressed trees. Similarly, girdled trees have been shown to first use younger NSC before remobilizing progressively older reserves (Muhr *et al.*, 2018). The relevance of these competition-related differences in tree vigor or girdling to trees experiencing drought stress is unclear: Do trees experiencing drought use their youngest NSC reserves first? This observation would be consistent with 'last in, first out' dynamics presented by Lacointe *et al.* (1993), in which the youngest NSC is the most accessible and/or the most abundant, and thus the first to be used under stress.

Mirroring global increases in drought frequency, duration, and severity, we compared a decade-long drought manipulation to a short-term, intense drought manipulation to understand how long-term drought stress impacts tree carbon reserves. We quantified NSC concentrations (sugars and starch) in all tissues (needles, twigs, sapwood, and roots) and $\Delta^{14}C$ in mature piñon (*Pinus edulis*) under both a long-term (> 10 yr, 45% precipitation removal) drought treatment and an extreme short term (*c.* 1 yr, 90% precipitation removal) manipulation. While crown NSC concentrations are typically the focus of global change experiments, we focused on bole sapwood because the majority of tree NSC resides in woody tissues (Hoch *et al.*, 2003). We specifically asked: how are trees' carbon reserves altered by long-term increases in drought stress?

Consistent with previous work (Carbone *et al.*, 2013; Muhr *et al.*, 2018), we hypothesized that (H1) drought-induced carbon starvation would increase the age ($\Delta^{14}C$) of the sapwood NSC pool as trees respire the youngest, readily available NSC first. We also hypothesized that (H2) trees that had experienced long-term drought (10 yr of 45% removal) would thus have an older (higher $\Delta^{14}C$) NSC pool than trees experiencing only a year of extreme drought (90% removal). To investigate what mechanisms underlie drought-induced changes in NSC pool age, we also measured a suite of physiological metrics, including water potential, photosynthesis, crown growth, chlorophyll fluorescence, bole respiration, tree-ring widths, and the age (^{14}C) of bole respired CO_2. We sought to improve our physiological understanding of the process, thresholds, and timescales of carbon starvation, which may underlie persistent impacts of drought upon tree growth (Peltier & Ogle, 2020).

Materials and Methods

Study site

The study site is located at 1910 m in the Los Piños mountains within the Sevilleta National Wildlife Refuge and Long-term Ecological Research (LTER) site, in south-central New Mexico, USA. The site is near the lower elevation limit of piñon pine (*Pinus edulis* Engelm.) in this range. Long-term mean annual precipitation is 347 ± 15 mm (1988–2015) and mean annual temperature is 14.5 ± 0.7°C (Sevilleta LTER Cerro Montoso station #42, elevation 1976 m, 2.2 km from site), and conditions at the site micrometeorological station were similar during 2019–2021 (Supporting Information Fig. S1). Roughly half of annual precipitation falls in winter, and half falls between July and September following a pronounced seasonal dry period from April to June. Certain years in the past decade have been among the warmest and driest on record (Williams *et al.*, 2020, 2022).

Plot design and study trees

In January 2020, two plots (*c.* 0.5 ha) were created, where precipitation exclusion structures covered *c.* 90% or 0% (control) of

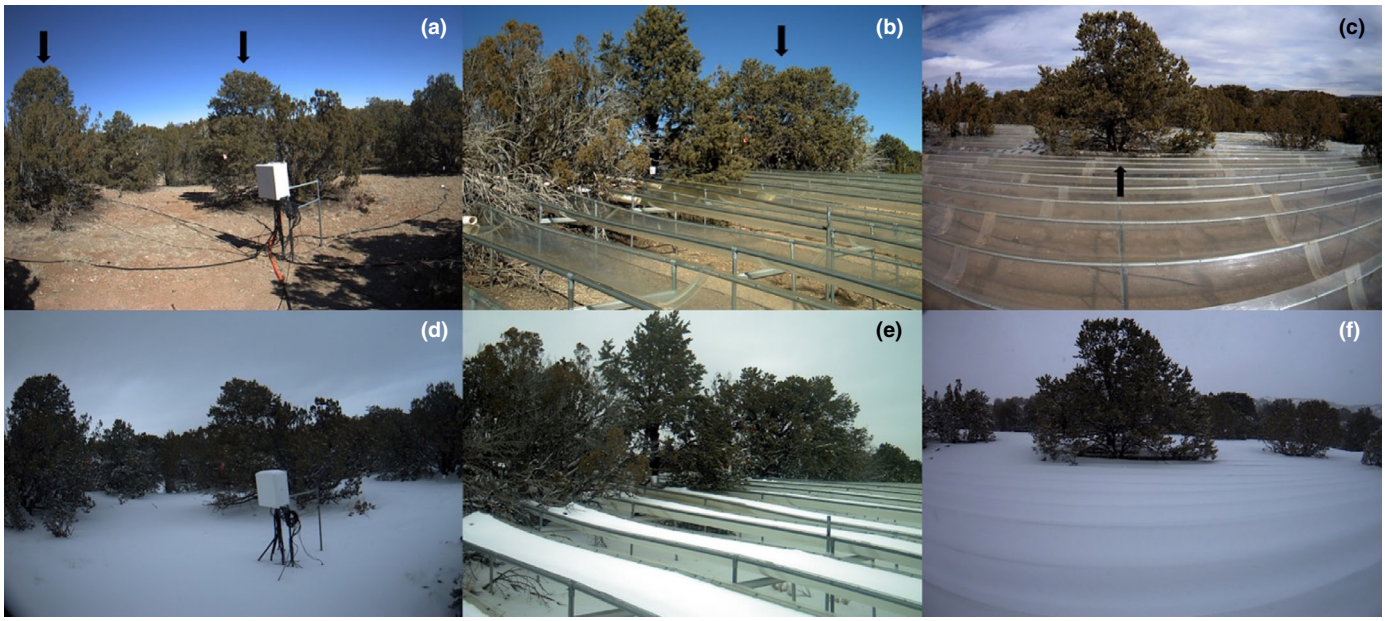

Fig. 1 Images of the control (a, d), legacy 45% rainfall exclusion (b, e), and 90% rainfall exclusion (c, f) plots under varying weather conditions during February 2021. A subset of focal *Pinus edulis* trees are also visible (black arrows). Study period images are freely available at https://phenocam.nau.edu (plots 16, 13, and 17). Treatment intensity (45% or 90%) refers to the area of the plot covered by plastic troughs (45% or 90% of plot area) where the remainder is uncovered (55% or 10%). Trees were similarly sized across plots, with mean diameter at 30 cm above ground of 20.6 ± 6.8 cm (control), 19.8 ± 6.8 cm (legacy 45%), and 19.2 ± 6.0 cm (90%).

the plots. A third plot was established in 2010 during a previous experiment (Pangle *et al.*, 2012) excluding *c.* 45% of incoming precipitation (Fig. 1). This third plot (hereafter 'legacy 45%') represents a long-term drought treatment on surviving trees. Trees in this plot were sprayed with insecticide (DragNet SFR, permethrin-based) from 2010 to 2015 following a bark beetle (*Ips confusus*) outbreak (Plaut *et al.*, 2012), but this plot went largely unmonitored from 2011 to 2019 (but see Dickman *et al.*, 2015). All plots follow Pangle *et al.* (2012), using large transparent plastic troughs below the crown to intercept and divert precipitation. Crown measurements focused on six *P. edulis* trees per plot, each at least five meters from plot edges. A subset of these trees (three per plot) was selected for measurements of NSC, ^{14}C, and bole CO_2 fluxes. One tree in the control plot died and was replaced with a similarly sized tree during fall 2020. With one plot per drought level this design might be considered pseudoreplicated, however, plots are large enough that trees are far apart and numerous previous studies (e.g. Pangle *et al.*, 2012; Adams *et al.*, 2015; McDowell *et al.*, 2019; Trowbridge *et al.*, 2021) have used this design. Finally, we explicitly account for within-plot similarity of trees using hierarchical Bayesian models, reducing maximum across-plot differences.

Soil moisture and ambient temperature monitoring

Soil volumetric water content (VWC, $m^3\ m^{-3}$) was measured at 30-min intervals in four pits within 15 m of plot center using EC-5 sensors (Decagon Devices, Pullman, WA, USA). Stratification of the pits captured heterogeneity of VWC under crowns and within gaps, and under and between plastic troughs. Three depths were measured in each pit at 10, 30, and 60 cm (thus, 12 per plot). Sensors were installed in spring of 2019 using a hand auger and inserting sensors horizontally. Soil horizons were visually separated then repacked to maintain stratification and bulk density. Ambient air temperature (°C) was measured using 24-gauge Type-T thermocouples (Omega, Stamford, CT, USA) 10 cm above the soil and shielded from sunlight. Similar to VWC stratification, 12 thermocouples were distributed among crown and intercrown space and under and between troughs within 15 m of plot center. All sensors connected to a CR1000 datalogger through AM16/32 and AM25T multiplexers (Campbell Scientific, Logan, UT, USA).

Leaf-level physiological monitoring

We monitored crown physiological metrics in the six study trees per plot at either monthly intervals (water potential and crown growth) or during peak growing season (May, June, and August; leaf gas exchange, crown NSC) from June 2019 to November 2021. We measured water potential at predawn (collected between 60 and 0 min before dawn) and mid-day (collected between 11:00 h and 12:30 h) using a Scholander-type pressure chamber (PMS instruments, Albany, OR, USA). Clipped twigs were kept in Ziploc bags in darkened coolers for up to 90 min between collection and measurement. We also quantified monthly growth following the methods of Adams *et al.* (2015). Using two twigs per tree, we measured terminal shoot length (from last bud scar) and needle growth monthly from May 2020 to November 2021.

Net photosynthetic rate (A_{net}) was quantified with a LiCor-6800 system (Lincoln, NE, USA) with small light source chamber (#6800-23) during June and August 2019, and May, June,

and August of 2020–2021 in the morning hours (07:00 h–10:00 h). Partial-sun exposed current year needles (youngest cohort) from each tree were measured under chamber conditions set to 400 ppm CO_2 and 2000 μmol m^{-2} s^{-1} PPFD. Temperature and humidity conditions were matched to those of the outside environment, where temperature was often *c.* 25°C and humidity *c.* 30%. A_{net} was corrected per unit leaf area using scanned images and IMAGEJ (imagej.nih.gov) and the LEAFAREA package (Katabuchi, 2015) in R (R Core Team, 2022).

Additionally, following observations of unusual needle color (yellowing) of 2020 needle cohorts in the 90% plot, we assessed drought impacts on the photosynthetic process. Thus, we quantified dark-adapted leaf chlorophyll fluorescence (F_v/F_m) using an Opti-Sciences OS-30p (New Hampshire, USA) handheld fluorometer. This measures maximum quantum yield of PSII; declines indicate photo-inhibitory damage as a result of temperature or water stress (Gamon & Pearcy, 1989; Epron *et al.*, 1992; Maxwell & Johnson, 2000). Measurements were conducted 1 h after sunset (i.e. darkness), monthly from March 2021 to June 2021 on 2020 needles on 10–20 twigs per tree. Monthly variation was small, so data were averaged within treatments.

Bole chambers to quantify respiration

Three trees in each plot were equipped to measure bole respiration. After leveling the bark surface with a draw knife, bole chambers (1.7 ± 0.25 l; determined by addition of known volume of reference gas) were affixed in September 2019 (Fig. S2). Chambers were affixed at heights between 0.1 and 1.3 m above the soil surface where suitably large surfaces were available and were below bole forks when possible. Thus, height and aspect varied. Chambers comprised 10.2 cm diameter ABS (acrylonitrile butadiene styrene) pipe beveled to fit the bole, with a 10.2 cm female adapter with a threaded lid. Lids were made from 10.2 cm ABS cleanout plugs drilled to accommodate two 0.64 cm bulkhead fittings (#PP1208E; John-Guest, West Drayton, UK). Chambers were affixed to boles with hot glue in September 2019, and if necessary, exterior sealed with an outer layer of silicone caulking. Chambers were checked before measurements for leaks and periodically externally re-caulked. Chambers were wrapped in reflective covering and left open between sampling.

Measurement of bole respiration rates

We used a closed chamber approach and a Flux Puppy system fully described in Carbone *et al.* (2019). The chamber was sealed with lid inlet and outlet ports attached to the Flux Puppy with tubing. Air from the chamber was circulated at *c.* 1 l min^{-1}, and CO_2 concentration was logged at 1-s intervals for 2–5 min depending on flux rates. Logged concentrations were fitted via linear regression in R (R Core Team, 2022) to quantify the increase. Nonlinear portions of curves were excluded, and coefficients of determination (R^2) were > 0.95. Resulting slopes (d[CO_2]/dt) were used to estimate CO_2 flux rate (R_{bole} in μmol CO_2 m^{-2} s^{-1}) from the bole surface as:

$$R_{bole} = \frac{d[CO_2]}{dt} \frac{V}{A} \frac{P}{RT} \quad \text{Eqn 1}$$

where V is chamber volume (L), A is surface area in the chamber (m^2), P is atmospheric pressure (atm), R is the universal gas constant (L atm K^{-1} mol^{-1}), and T is chamber air temperature (K). Temperature was measured through a sealed port. Because the temperature at which each measurement was taken was variable across seasons and time of day, we fit a temperature model to temperature-correct means across trees and treatments. We fit a hierarchical mixed effects model with random slopes and intercepts (tree- within plot-level) with temperature as a covariate, and predicted mean (plot-level) respiration rate at 21.7°C (mean temperature in the control plot). This was done in a Bayesian framework (Methods S1).

$\Delta^{14}C$ of respiration CO_2

$\Delta^{14}CO_2$ was collected from boles three times (March, June, and November 2020) following Carbone *et al.* (2013). Lids were placed on bole chambers in the early morning and accumulated CO_2 for *c.* 8–24 h depending upon ambient temperatures. We do not account for diurnal dynamics, seeking only to achieve sufficient CO_2 concentrations. Chamber gas was collected with a pump onto zeolite traps (Hardie *et al.*, 2005), or with previously evacuated air stabilizer cans (X21L-1002; LabCommerce, San Jose, CA, USA). Cotemporaneous atmospheric samples were collected using 6-l stabilizer cans to correct $\Delta^{14}CO_2$ for ambient air in the chamber.

$\Delta^{14}C$ of sapwood NSC

Increment cores were collected annually (2019 and 2020) in November. To enable subsampling, a 12-mm diameter borer (Mattson, Sweden) was required to sample the main bole (^{14}C cores). Replicate 5.15-mm cores were collected for NSC concentration measurements (NSC cores). The NSC cores were immediately frozen on dry ice upon removal from the tree. The ^{14}C cores were temporarily mounted in the field on a vice with sanitized contact surfaces, where a level surface was cut with a clean razor blade to visualize ring boundaries. Active sapwood depth was determined as the deepest hydrated ring, and the sapwood was then split into radial thirds (by depth, not ring count). These thirds are subsequently referred to as shallow (outside third), medium (middle third), and deep (third up to the sapwood-heartwood boundary) sapwood.

These three sapwood subsamples (^{14}C cores) were then placed in sealed custom 256 ml Mason jars with modified two-port lids (Luer-lock fittings with valves). Chambers were initially purged of atmospheric CO_2 (using a pump and soda-lime column), where previous work showed this successfully removes *c.* 99% of atmospheric CO_2. Thus, headspace air collected after 120 h represents respired carbon from respiration of live cells within the wood drawing upon stored carbon reserves, that is,

NSC (Hilman *et al.*, 2021; Peltier *et al.*, 2023). Subsequently, headspace air was collected after 120 h onto previously evacuated 1-l gas-stabilizer cans (X31L-1004; LabCommerce, CA, USA) for preparation to measure ^{14}C (analytical steps described below).

Finally, for each tree, *t*, we also calculated the mean age of the total available NSC pool $\overline{Age}_t$, taking a mass-weighted average according to the respired carbon totals from incubations (CO_2 produced, 'mass') at each sapwood depth (shallow, medium, and deep), *d*, as:

$$\overline{Age}_t = \sum_{d=1}^{3} Age_{t,d} \times mass_{t,d} \quad \text{Eqn 2}$$

To test for treatment differences in total NSC ^{14}C ages, we fit a hierarchical linear model with year and treatment as factors to estimate a latent year-independent mean for each plot (Methods S1).

Furthermore, we approximated the composition and turnover time of total NSC using a two-pool model (Richardson *et al.*, 2015). We performed simulations using the 'SOILR' package (Sierra *et al.*, 2012) to trace carbon through multiple pools and account for radioactive decay. Because we have no NSC data during 2011–2019 (but see: Dickman *et al.*, 2015), we assumed steady state in these simulations. It is possible legacy 45% plot trees were not at steady state, but we have no 2011–2019 NSC or gas exchange data to constrain a more sophisticated nonsteady-state model (e.g. Metzler *et al.*, 2018; Herrera-Ramírez *et al.*, 2020). Mean age only approximates turnover time only under steady state, but a steady-state model is still useful to contextualize possible changes in NSC pools. We used a range of turnover times (1–60 yr) and relative pool sizes (slow pool from 1 to 99% of total) to generate 11 781 candidate NSC mixtures to which we matched the mean total sapwood NSC ages observed in our plots. More details are provided in Methods S2.

Measurement of ^{14}C via accelerator mass spectrometry

CO_2 from bole respiration and sapwood incubation samples was subsequently purified and converted to graphite following standard preparation methods (Lowe, 1984; Vogel *et al.*, 1984) for accelerator mass spectrometry (AMS) and analyzed at the UC Irvine Keck AMS facility or on a MIni CArbon DAting System (MICADAS, IonPlus, Switzerland; Synal *et al.*, 2007) at the Arizona Climate and Ecosystems (ACE) Laboratory at Northern Arizona University.

The data (decay-corrected $\Delta^{14}C$) are reported as per mil (‰) following standard methods (eqn 3.19 in Trumbore *et al.*, 2016). Modern standards (Oxalic acid II) run at both AMS facilities had a standard deviation of ±2‰. We estimated sample ages (years since fixation) from $\Delta^{14}C$ by comparing with an atmospheric bomb curve for the northern hemisphere (NH2, Hua *et al.*, 2022). To verify that our site atmosphere $\Delta^{14}C$ matched this record, we analyzed the $\Delta^{14}C$ of archived (from 2013, 2014, and 2018) and collected (from 2020) annual plant tissue, which did fall directly onto the northern hemisphere zone 2 record (Fig. S3).

NSC concentration measurements

NSC cores (flash-frozen after collection) were freeze-dried, subsectioned to match sectioning of the ^{14}C cores, and ground on Retsch ball mill (Retsch MM 200 ball mill, Haan, Germany) to a fine powder. Samples were subsequently analyzed following the standard phenol-sulfuric acid method (Landhäusser *et al.*, 2018) as in Furze *et al.* (2019). In this method, NSC concentrations of both sugar and starch fractions are measured following extractions via color formation with reference to a standard curve using a spectrophotometer (GENESYS 10S UV–Vis; Thermo Fisher Scientific, Waltham, MA, USA). To test for changes in NSC concentrations with sapwood depth, we fit hierarchical linear regressions to sugar and starch concentration data in a Bayesian framework (Methods S1). To test for treatment differences in starch concentrations, we fit a hierarchical linear model with year and treatment as factors (Methods S1).

We similarly measured NSC concentrations in needles and twigs, and coarse roots during our study (2019–2021), before which the legacy 45% plot went unmonitored for years. Because root coring is potentially destructive, coarse root samples were collected annually using 5.15 mm increment cores, June 2019–2020. While NSC cores were flash-frozen in the field and subsequently freeze-dried (described above), crown and root NSC samples were microwaved for 180 s after collection and subsequently dried in a drying oven at 60°C for 48 h.

Ring width measurements

We also measured ring widths on the nine study trees (three per plot) on which we measured ^{14}C and NSC, plus an additional four trees located adjacent to plots. For study trees, we measured ring widths on the ^{14}C cores collected in November 2020 as described above. These cores were sanded with increasingly fine-grain sandpaper to clearly visualize ring boundaries. For off-plot trees, we collected 5.15-mm increment cores in June 2021, these were similarly dried, mounted, and sanded. Cores were visually cross-dated following standard methods (Fritts & Swetnam, 1989). Ring widths were measured on a sliding stage (Velmex, Bloomfield, NY, USA) via the measure J2X software (VoorTech Consulting, Holderness, NH, USA). Cross-dating was statistically assessed with the DPLR package (Bunn, 2008) in R. Ring widths were converted to basal area increment (BAI) using root collar diameter (30 cm above the soil) to remove geometric growth trends (Biondi & Qeadan, 2008). All cores sampled for ^{14}C, NSC, and ring width were collected below 60 cm height.

Other statistical comparisons

To assess treatment differences among plots when data were not normally distributed (predawn water potentials in September 2020 and June 2021, post-2019 A_{net}, and end of study needle and shoot lengths), we used Dunn's test following a Kruskal–Wallis test. To assess treatment differences in leaf fluorescence, we used Tukey's honest significant difference test following one-

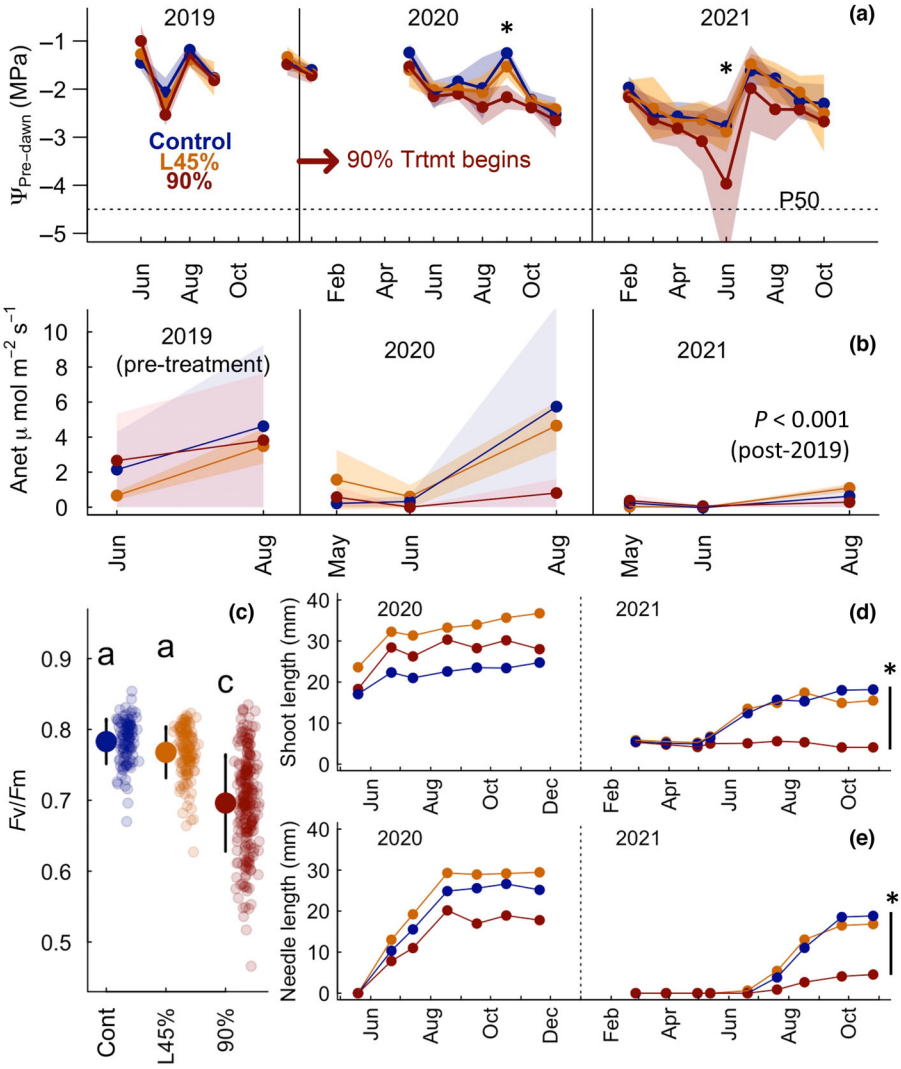

Fig. 2 Crown physiological metrics during the course of the experiment. (a) Predawn water potential, Ψ_{PD} (b) photosynthesis, A_{net} (c) chlorophyll fluorescence, F_v/F_m (d) shoot growth and (e) needle growth in the control (blue), legacy 45% (orange), and 90% (red) plots. The 90% plot was fully completed around January 2020. P50 for *Pinus edulis* from Hudson *et al*. (2018). Mean ± SD ((a, b) lines and shading, (c) circles, and vertical black lines) are shown. In (a), '*' denotes 90% plot Ψ_{PD} was significantly lower than the control in September 2020 and June 2021 (Dunn's following Kruskal–Wallis: $P < 0.05$). In (b), post-2019 A_{net} was significantly reduced in the 90% plot (Dunn's following Kruskal–Wallis: $P < 0.001$). In (c) March–June 2021 F_v/F_m was reduced in the 90% plot, lower case letters denote significant differences (Tukey HSD following ANOVA: $P < 0.05$; total $n = 483$). In (d, e) '*' denotes late-2021 needle and shoot growth were significantly reduced in the 90% plot (Dunn's following Kruskal–Wallis: $P < 0.01$) where uncertainty bands are omitted because variation (within-plot) was very large.

way ANOVA. To test for changes in radial growth following construction of the legacy 45% plot, for each tree, we compared mean BAI before 2011, and from 2011 to 2020. Because there were no clear effects of the 90% treatment on 2020 ring width (many trees both on and off plot were missing 2021 rings due to ambient drought), we then averaged these indices (BAI pre-2011 and BAI 2011–2020) across (1) legacy 45% plot trees and (2) all other measured trees, and we compared these two quantities with a *t*-test.

Results

Over the entire study period, drought treatments decreased soil VWC compared with the control (Fig. S4). Due to long dry periods and large, saturating summer rain events (Fig. S1), temporal variation was large: legacy 45% and 90% treatment plots had VWC of 0.12 ± 0.14 m^3 m^{-3}and 0.11 ± 0.10 m^3 m^{-3}, respectively (control: 0.14 ± 0.14 m^3 m^{-3}). But water potentials show drought treatments were highly effective at peak water stress (late summer, Fig. 2a); two of six study trees also died in the 90% plot in summer 2021. These structures also had a slight warming effect, with mean temperatures of 17.3°C and 19.2°C, in the legacy 45% and new 90%, respectively, relative to 16.2°C in the control plot (Fig. S4).

Impaired crown physiology in short-term drought plot

Four ecophysiological metrics showed clear impacts on crown physiology in the 90% treatment, but not in the legacy 45% plot (Fig. 2). First, predawn water potentials in the control and legacy 45% plots were similar across the study, with most measurements between −1 and −3 MPa, and more negative water potentials in peak growing season (Fig. 2a). By contrast, compared with the control, water potentials in the 90% plot were similar in 2019 (pretreatment), but significantly more negative in September 2020 and June of 2021 ($P < 0.05$, Fig. 2a). In June 2021, the 90% plot mean approached P50 (*c.* −4.4 MPa)—the water potential at which 50% of stem conductivity is lost to embolism – for *P. edulis* (Hudson *et al.*, 2018), after which two trees were attacked by beetles and died.

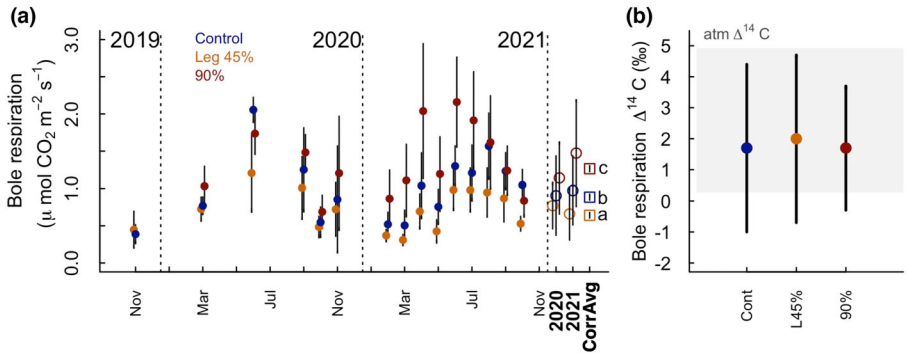

Fig. 3 Respiration fluxes and the age of respired carbon measured in bole chambers. (a) Monthly bole respiration fluxes (mean ± SD) in *Pinus edulis* for the control (blue-filled circles), legacy 45% (orange-filled circles), and 90% (red-filled circles) over November 2019–November 2021 (jittered). Plot-level 2020 and 2021 mean ± SD (unfilled circles and lines) and overall temperature-adjusted means ('CorrAvg', unfilled squares and lines) are also presented. Temperature-adjusted means are predicted flux at 21.66°C (mean temperature in the control plot), where lowercase letters indicate significant differences ($P < 0.001$). (b) Bole respiration flux $\Delta^{14}C$ for each plot (2020 mean ± SD) and observed site $\Delta^{14}C$ local atmosphere (gray shading; 2020 annual plant $\Delta^{14}C = 2.6 \pm 2.3‰$).

Second, the 90% treatment essentially halted leaf gas exchange compared with the control or legacy 45% plots in 2020, before extremely dry ambient conditions in 2021 ($P < 0.001$, Fig. 2b). Mean A_{net} in the legacy 45% plot remained similar to the control throughout the study period, though all plots showed reduced gas exchange through most of 2021 due to a dry spring and preceding fall (Fig. 2b; and note lower water potentials across plots in 2021, Fig. 2a). Ambient conditions in late-2020 into early-2021 in the southwestern United States were consistent with the worst drought in 1200 yr (Williams *et al.*, 2022), and this resulted in very little gas exchange in any study trees in summer of 2021.

Third, chlorophyll fluorescence (F_v/F_m) in the 90% plot in spring of 2021 was reduced (0.70 ± 0.06) in 2020 needle cohorts ($P < 0.05$, Fig. 2c) consistent with observed yellowing. A 'normal' value of F_v/F_m might be *c.* 0.8 (Maxwell & Johnson, 2000), matching the values observed in the control (0.78 ± 0.03) and legacy 45% (0.78 ± 0.03) plots, where legacy 45% plot F_v/F_m was indistinguishable from the control. By contrast, values of F_v/F_m near 0.5 were observed in some trees in the 90% plot. In another study, similar values required treatment of conifer needles at temperatures exceeding 45°C (Kunert *et al.*, 2021).

Fourth, trees in the 90% plot showed reduced and delayed shoot and needle elongation, particularly in 2021, compared with the control or legacy 45% ($P < 0.01$, Fig. 2d,e). For most trees, shoot elongation began in May and terminated in September, while budbreak was initiated in June (2020) or July (2021) and needle maturity was reached in August (2020) or September (2021). However, in the 90% plot, mean shoot and needle lengths never exceeded *c.* 5 mm for the duration of the 2021 growing season, and some twigs died. Mean 2021 peak needle length in other plots was *c.* 15 mm. In 2021, needle growth also initiated at least 1 month later in the 90% plot, compared with the control and legacy 45% plot. Despite these physiological impacts of the 90% treatment, we found no significant differences in sugar or starch concentrations among treatments, or effects of the 90% treatment, in needles, twigs, or coarse roots ($n = 594$, Fig. S5). There were suggestive declines in root NSC, but sample sizes were smaller for this tissue (annually collected), and differences were not significant (Fig. S5).

Reduced respiration rates in long-term drought plot

Bole respiration rates showed comparable seasonal trends across all three plots, with higher fluxes in the warmer (summer) months (Fig. 3a). But temperature-corrected (to 21.66°C) respiration rates were significantly higher in the 90% plot (143% of control, $P < 0.01$), particularly in 2021 (Fig. 3a, squares). Respiration rates were significantly lower in the legacy 45% plot (71% of control, $P < 0.01$). Despite these large differences, bole respiration $\Delta^{14}C$ was similar across plots and season during 2020. The mean $\Delta^{14}C$ of respiration was similar to atmospheric $\Delta^{14}CO_2$ (quantified by the annual plants; 2.6 ± 2.3‰) showing that the trees are respiring carbon that is 0–1 y old across all plots (Fig. 3b).

Reduced radial growth age in long-term drought plot

Reduced bole respiration rate under long-term drought was also reflected in reduced radial growth by 39% compared with the undroughted trees ($P < 0.001$, Fig. 4a). While all trees showed reduced BAI compared with pre-2011 means, in the legacy 45%, plot 2011–2020 BAI was only 32% of pre-2011 values (Figs 4a, S6). By contrast, undroughted trees 2011–2020 BAI was 72% of pre-2011 values. Missing (locally absent) rings were also common (Fig. 4b), where *c.* 25% of 2011–2020 rings were missing in the three legacy plot trees (eight of 30 total rings). In comparison, only 6% of rings were missing in the undroughted trees during this same period (six of 100 rings).

Reduced starch concentrations in long-term drought plot

Sapwood soluble sugar concentrations did not differ between plots or sampling year, and all trees showed declining sugar concentrations with increasing sapwood depth ($P < 0.05$, Fig. 5a). Sapwood starch concentrations were unrelated to depth and there

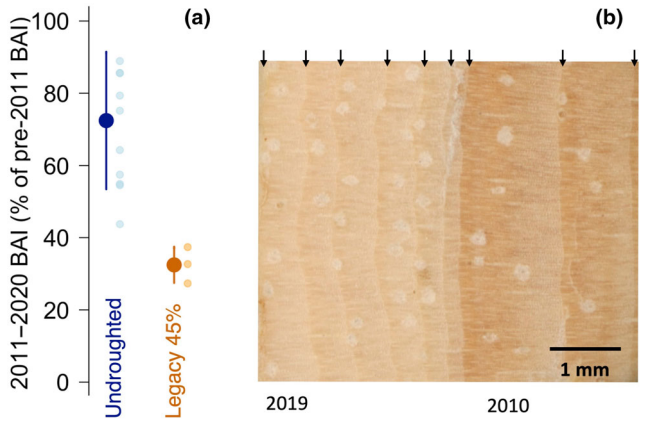

Fig. 4 Radial growth characteristics of legacy 45% plot trees as compared to undroughted trees. Shown in (a) are mean basal area increment (BAI) for the decade 2011–2020 as a percent of previous BAI for each *Pinus edulis* tree (small circles) and mean ± SD undroughted (large blue circles, lines) and legacy 45% trees (large orange circles, lines). Also shown are (b) the most recent 12 yr of growth in a tree in the legacy 45% plot as of November 2019, showing reduced growth where 3 rings (likely 2011, 2013, and 2018) are missing after treatment began; arrows denote ring boundaries. In (a), because no effects of 90% drought were evident in the one post-treatment tree ring available (2020), tree-level values were aggregated to 'undroughted' trees ($n = 10$; control and 90%, plus four off-plot trees) and legacy 45% plot trees ($n = 3$). These two groups of trees % change in BAI were completely nonoverlapping (*t*-test: $P < 0.0001$). Full tree-ring width dataset is shown in Supporting Information Fig. S6.

were no effects of year of sampling (Fig. 5b), but mean sapwood starch concentrations differed significantly across plots ($P < 0.05$) and were sometimes indistinguishable from zero in the legacy 45% plot (Fig. 5c). In November 2019, sapwood starch concentrations were *c.* 75% lower in the legacy 45% plot than either the 90% (pretreatment) or the control ($P < 0.05$). Sapwood starch concentrations in the legacy 45% plot remained unchanged in November 2020. In the 90% plot, there was no clear treatment effect on starch after 1 yr (Fig. 5c). Total sapwood NSC in 2019 were on average 2.7 ± 1.7 mg in the legacy 45% plot (77% of control), compared with 3.5 ± 0.7 mg in the control plot and 3.8 ± 1.3 mg in the 90% plot.

Reduced NSC age in long-term drought plot

In 2019 and 2020, sapwood NSC age (based on ^{14}C measurements) increased with depth up to the heartwood boundary ($P < 0.001$, Fig. 6a) across plots. NSC age was unrelated to any crown physiological metrics we explored (e.g. water potential, A_{net}, chlorophyll fluorescence; Fig. S7). NSC age in shallow sapwood across all plots ranged from 1.8 ± 0.5 to 6.2 ± 0.5 yr, while the range in deep sapwood was much larger, from 3.5 ± 0.5 to 20.5 ± 0.4 yr. NSC ages across plots showed similar patterns, except trees in the legacy 45% plot tended to have younger NSC in deep sapwood compared with trees in other plots. Comparing mean total sapwood NSC age across plots and years, we found total NSC age was significantly lower in the legacy 45% plot (4.1 ± 1.4 yr) compared with the control (7.3 ± 0.9 yr; $P < 0.05$, Fig. 6b). Total sapwood NSC age in the legacy 45% plot was reduced by 44% from the control. Calculating this same ratio directly within the mixed effects model (which accounts for tree-plot identity, Methods S1) gives a mean age reduction of exactly 50%. Further forward simulation modeling assuming steady state suggested this reduction in age ($\Delta^{14}C = 26.8$ to $\Delta^{14}C = 13.0$) is consistent with either reduction in the turnover time of the slow pool of sapwood NSC (mean of 6 yr shorter; range 3–32 yr shorter), reduction in the relative amount of slow pool NSC (mean of 16% less; range 12–51% less), or both (Fig. 6c). Both reduction in maximum age or reduction in old amount would reflect a loss of old NSC.

Discussion

Total tree NSC pools are large (Hoch *et al.*, 2003), and thus resilient to short-term stress. However, this is the first study to provide evidence that long-term drought can alter the ^{14}C age of

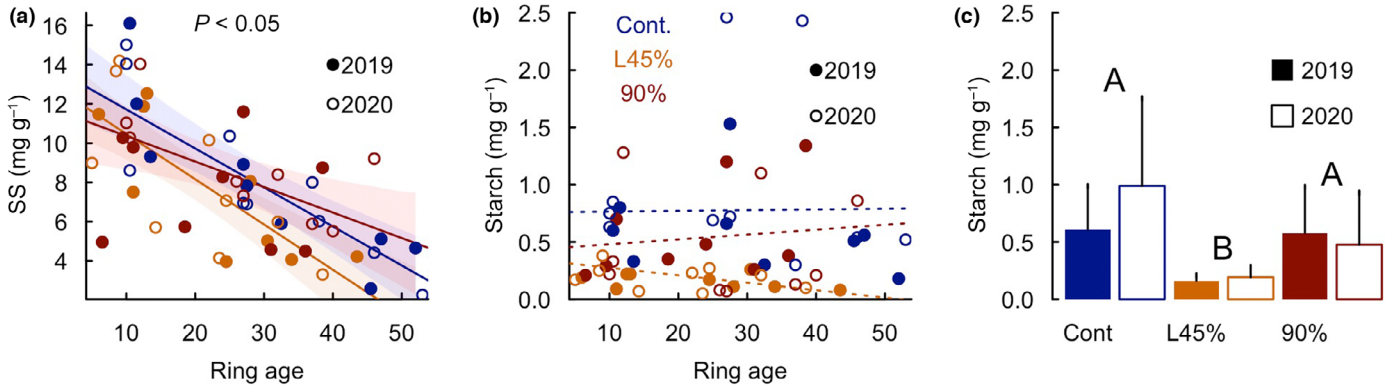

Fig. 5 Sapwood nonstructural carbohydrate (NSC) concentrations in study trees. (a) Soluble sugar and (b) starch concentrations are given for each radial third for November 2019 (filled circles) and November 2020 (unfilled circles), where the ring age represents the middle ring of a given sapwood third for a given *Pinus edulis* tree. Colors denote control (blue), legacy 45% (orange), and 90% (red) plots. Sugar concentrations were significantly related to ring age in all plots (plot-level fits and 95% CrI shown as lines and shading), but did not vary across years (Hierarchical-Bayesian regression). Starch concentrations were unrelated to ring age, and so mean ± SD starch concentrations across all sapwood depths and trees are given in (c). Uppercase letters indicate significant differences among plots, where year effects were not significant (Hierarchical-Bayesian ANOVA). Note there were no significant differences in sugar or starch concentrations across treatments (or time periods) for needles, twigs, or coarse roots (Supporting Information Fig. S5).

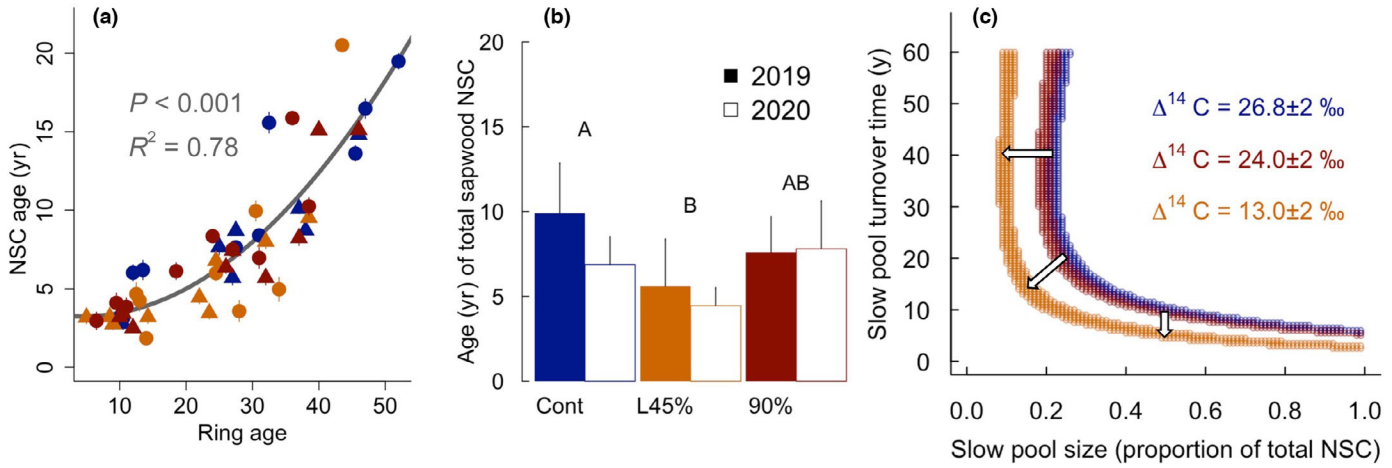

Fig. 6 Ages of sapwood non-structural carbohydrates (NSC) and associated model results. (a) Δ^{14}C-derived age of non-structural carbohydrates (NSC) (±accelerator mass spectrometry error) across sapwood depths in 2019 (circles) and 2020 (triangles) for the control (blue), 45% legacy (orange), and 90% (red) plots in *Pinus edulis* are shown. (b) Plot mean ± SD of tree-level mass-adjusted total NSC age in 2019 (filled bars) and 2020 (unfilled bars). (c) Two-pool steady-state model simulations ($n = 11\,781$) yielding total sapwood NSC ages matching each of the three plots in (b) shows how reduced age, reduced slow pool size, or both could result in reduced legacy 45% plot NSC ages (white arrows). In (a), a second-order linear model fit of NSC ^{14}C age on ring age across all observations is shown (gray line). In (b), uppercase letters denote significant differences after removing year effects ($P < 0.05$) in a hierarchical Bayesian linear model. Full Δ^{14}C dataset with reported in Supporting Information Table S1.

NSC pools stored in trees through the consumption of old reserves under carbon starvation. Future work in other species or contexts might identify whether 50% reduction in mean NSC age is typical, or whether larger reductions are possible. In the 90% plot, despite physiological impairment due to severe moisture stress (Fig. 2), trees' crown and sapwood NSC storage appeared resilient to extreme drought stress, at least in the short term. NSC concentrations, NSC ^{14}C ages, and the total ^{14}C age of the sapwood NSC pool were all indistinguishable from control trees in the 90% plot (Figs 5, 6, S5), despite increases in respiration rates (Fig. 3). NSC pools may have been maintained due to sink limitation following reduced canopy growth (Huang *et al.*, 2021) but growth and carbon uptake are often co-limited in this species (Thompson *et al.*, 2023). Regardless, this resiliency of NSC pools to even extreme drought should be considered in contextualizing global change experiments finding no clear impacts on NSC reserves from short-term treatments. Instead of concluding carbon starvation is rare, perhaps it only begins once trees have exceeded some threshold in duration (i.e. multiple years; He *et al.*, 2020; Wang *et al.*, 2020).

Then, carbon starvation takes time – measured in years, not months. Sapwood NSC concentrations, growth, and metabolism were impacted in trees experiencing a decade of drought, while similar responses were not evident after 1 yr of extreme drought. Sometimes in the past decade, trees experiencing long-term drought consumed sapwood starch pools (Fig. 5c; see also: Rowland *et al.*, 2021). More compelling was the large (39%) decrease in radial growth and the recent prevalence of missing rings after 2010 (Fig. 4). This reduction in growth was also reflected in reduced bole respiration rates (Fig. 3). These data are consistent with carbon starvation in trees surviving 45% precipitation removal for a decade (McDowell *et al.*, 2022). We suggest that by reducing growth and respiration rates with greater reliance on old NSC reserves, they have been able to survive (perhaps through regulatory changes; Huang *et al.*, 2021; Tsamir-Rimon *et al.*, 2021). These trees were sprayed with an insecticide from 2010 to 2015, perhaps allowing for a deeper drawdown of NSC pools than under other circumstances. ^{14}C measurements provide additional support for the interpretation that trees relied on old NSC, where, for example, forward simulations show reduction in the amount of old NSC or the age of the oldest NSC could produce the patterns we observed in Fig. 6.

Contrary to our hypothesis (H1), NSC in trees under long-term drought was younger, implying more rapid cycling (or turnover) of NSC than in control trees. Then, trees under long-term drought have relied more on storage, consuming older reserve carbon (Fig. 6c). If we assume early responses (*circa* 2010) matched those observed in the 90% plot here (Fig. 2b,c), trees under long-term drought were less capable of adding assimilates to their storage pool each year, particularly in initial treatment years, resulting in the process of carbon starvation whereby NSC pools are gradually reduced (McDowell *et al.*, 2022). In combination or in isolation, both increased respiratory consumption and reduced photosynthetic uptake could lead to a younger and smaller NSC pool (Fig. 6c), but reduced C uptake alone is probably insufficient to explain our results. While starch is often assumed to represent long-term (older) storage, sugar and starch pools exchange through interconversion at least seasonally (Furze *et al.*, 2019; Guo *et al.*, 2020; Tsamir-Rimon *et al.*, 2021) and thus tend to be of similar age (within the same tissue; Richardson *et al.*, 2013). Thus, given starch only represented 5–10% of the total NSC pool in these trees, characteristic of typically low sapwood starch in pines, even a total depletion of starch under long-term drought cannot explain the reduced total NSC ages (−44 to 50%) observed in the long-term drought plot (Fig. 6b). The remaining NSC (sugars) must have become younger. This indicates sugar pools in trees – while of similar concentrations to control trees – have also become younger under long-term drought

(Fig. 6c). As described earlier, ^{14}C measurements of NSC pools can detect changes in the cycling of carbon that may not be reflected in concentrations. Broader application of ^{14}C measurements of NSC may reveal new complexities in carbon starvation in response to drought and other stressors.

Other potential explanations for the altered NSC ages observed in the legacy 45% plot could be explored (e.g. irrelevance of old NSC or sink limitation), but carbon starvation leading to consumption of old reserves appears best supported. For example the relevance of very old NSC to physiological function has been questioned, as some of this NSC is eventually used to produce heartwood (Spicer, 2005). Yet, old NSC (up to 17 yr) can be remobilized after diverse disturbances (Vargas *et al.*, 2009; Carbone *et al.*, 2013; Muhr *et al.*, 2018; D'Andrea *et al.*, 2019), so trees under long-term drought may have access to their oldest reserves. Another potential explanation is long-term drought-induced sink limitation in these trees, leading to observed reductions in radial growth (Fig. 4). But given similar carbon uptake and hydraulic function to the control (Fig. 2), this type of growth limitation should then be associated with increased NSC concentrations (McDowell, 2011) and older NSC ages, when in fact, we see reductions in sapwood concentrations and age (Figs 5, 6), and similar concentrations elsewhere (Fig. S5). Initial sink limitation could explain resilience of NSC concentrations in the 90% plot (Fig. 5). But increases in NSC under drought are likely to be transient responses to moderate drought stress, where carbon starvation takes place once drought is sufficiently extreme and prolonged (He *et al.*, 2020).

Acclimation via other changes in canopy leaf area, belowground investment, or sapwood area may also have occurred in these trees to permit survival. First, hydraulic stress, canopy growth, and photosynthetic indices are identical to control trees – at the leaf level. NSC concentrations in leaves, twigs, and roots also do not significantly differ between plots (Fig. S5). But trees under long-term drought may have shed needles or branches over the past decade reducing total canopy water demand (Rood *et al.*, 2000). Even without losing needles, trees under long-term drought could have reduced canopy area due to sustained reductions in needle and twig growth (as in the 90% here, Fig. 2d,e) consistent with other studies (Adams *et al.*, 2015; Grossiord *et al.*, 2017). Second, trees may have increased investment in belowground water resources via root growth (Hagedorn *et al.*, 2016), though a modeling study leveraging observations from a similar drought experiment suggests root growth is both expensive and too slow to permit reasonably fast acclimation in this species (Mackay *et al.*, 2020). In this study, there was not clear evidence for differences in NSC ages in roots (Table S1). Third, trees may be limited by legacies of past hydraulic dysfunction in their xylem (Rood *et al.*, 2000; Hagedorn *et al.*, 2016; McDowell *et al.*, 2016; Trugman *et al.*, 2018; Rehschuh *et al.*, 2020). Most likely, a combination of such processes and others have all occurred throughout the past decade to scale back canopy water demand in response to reduced supply and provisioning capacity. We hypothesize reduced total crown leaf area following hydraulic damage or reduced (or delayed, Fig. 2d,e) canopy growth would be sufficient to explain observed acclimation of *leaf-level* crown physiology but continued perturbation of carbon metabolism in the sapwood (including no differences in crown NSC, Fig. S5, or stomatal conductance, Fig. S8). Acclimatory responses (including metabolism of old NSC) highlight how trees may exist in perturbed physiological states, while exhibiting apparently similar leaf-level physiology (Figs 2, S5).

Our data document carbon starvation comprising the loss of old sapwood NSC occurring in the legacy 45% after a decade of drought, while physiological impacts of the 90% treatment show a hypothetical pathway toward progressive carbon starvation under long-term drought. This cumulative, slow process may thus become quite common as trees continue to experience more pronounced and prolonged droughts across the landscape (Williams *et al.*, 2020). Given the often decisive role of bark beetles in drought-related mortality in conifers, including at this site (e.g. Plaut *et al.*, 2013), carbon starvation may increase subsequent vulnerability to mortality from bark beetles if defenses are also reduced (Trowbridge *et al.*, 2021; Monson *et al.*, 2022). *Pinus edulis* is relatively drought-adapted – other pine species might experience rapid hydraulic failure or lethal carbon starvation even when protected from beetles. Our mechanistic physiological framework also highlights drought must be sufficiently intense and prolonged to observe carbon starvation (He *et al.*, 2020), perhaps after transient sink limitation. We conclude a year of extreme drought is insufficient to impact NSC reserves, but perhaps a single favorable year would be insufficient to replenish old NSC pools drawn down over more than a decade of drought.

Acknowledgements

We thank Lauren Baur, Renee Brown, and Don Natvig at the Sevilleta LTER, Michael Friedman for assistance with field monitoring, Chris Ebert and Kiona Ogle at NAU, and Xiaomei Xu at UC Irvine. We gratefully acknowledge the financial support of the Office of the President and Vice President of Research at Northern Arizona University for support in acquiring the MICADAS. This work was funded by the NSF via IOS-RAPID-1936205, IOS-1755345, and IOS-1755346, and NSF GRFP 1-842493. HDA was also supported by the US Department of Agriculture, National Institute of Food and Agriculture, McIntire Stennis project 1019284.

Competing interests

None declared.

Author contributions

AMT, HDA, WTP, NM and CDM designed the drought study. CDM, NR, DMPP, RAT, SM, HDA, WTP, NGM, JL and AMT collected the data. DMPP conducted respiration and radiocarbon measurements with significant input from MSC and ADR. DMPP analyzed the data. DMPP and MSC wrote the first draft of the manuscript. All authors contributed significantly to revisions.

ORCID

Henry D. Adams https://orcid.org/0000-0001-9630-4305
Mariah S. Carbone https://orcid.org/0000-0002-7832-7009
Shealyn Malone https://orcid.org/0000-0002-8241-181X
Nate G. McDowell https://orcid.org/0000-0002-2178-2254
Cameron D. McIntire https://orcid.org/0000-0001-9666-5805
Drew M. P. Peltier https://orcid.org/0000-0003-3271-9055
William T. Pockman https://orcid.org/0000-0002-3286-0457
Andrew D. Richardson https://orcid.org/0000-0002-0148-6714
R. Alex Thompson https://orcid.org/0000-0001-5761-1038
Amy M. Trowbridge https://orcid.org/0000-0001-8993-2530

Data availability

All data are archived on Zenodo: https://zenodo.org/record/7972162.

References

Adams HD, Collins AD, Briggs SP, Vennetier M, Dickman LT, Sevanto SA, Garcia-Forner N, Powers HH, McDowell NG. 2015. Experimental drought and heat can delay phenological development and reduce foliar and shoot growth in semiarid trees. *Global Change Biology* **21**: 4210–4220.

Adams HD, Zeppel MJ, Anderegg WR, Hartmann H, Landhäusser SM, Tissue DT, Huxman TE, Hudson PJ, Franz TE, Allen CD. 2017. A multi-species synthesis of physiological mechanisms in drought-induced tree mortality. *Nature Ecology & Evolution* **1**: 1285–1291.

Anderegg WR, Anderegg LD. 2013. Hydraulic and carbohydrate changes in experimental drought-induced mortality of saplings in two conifer species. *Tree Physiology* **33**: 252–260.

Anderegg WR, Trugman AT, Badgley G, Konings AG, Shaw J. 2020. Divergent forest sensitivity to repeated extreme droughts. *Nature Climate Change* **10**: 1091–1095.

Anderegg WRL, Schwalm C, Biondi F, Camarero JJ, Koch G, Litvak M, Ogle K, Shaw JD, Shevliakova E, Williams AP *et al.* 2015. Pervasive drought legacies in forest ecosystems and their implications for carbon cycle models. *Science* **349**: 528–532.

Biondi F, Qeadan F. 2008. A theory-driven approach to tree-ring standardization: defining the biological trend from expected basal area increment. *Tree-Ring Research* **64**: 81–96.

Blumstein M, Sala A, Weston DJ, Holbrook NM, Hopkins R. 2022. Plant carbohydrate storage: intra-and inter-specific trade-offs reveal a major life history trait. *New Phytologist* **235**: 2211–2222.

Bonan GB. 2008. Forests and climate change: forcings, feedbacks, and the climate benefits of forests. *Science* **320**: 1444–1449.

Bunn AG. 2008. A dendrochronology program library in R (DPLR). *Dendrochronologia* **26**: 115–124.

Carbone MS, Czimczik CI, Keenan TF, Murakami PF, Pederson N, Schaberg PG, Xu X, Richardson AD. 2013. Age, allocation and availability of nonstructural carbon in mature red maple trees. *New Phytologist* **200**: 1145–1155.

Carbone MS, Seyednasrollah B, Rademacher TT, Basler D, Le Moine JM, Beals S, Beasley J, Greene A, Kelroy J, Richardson AD. 2019. Flux Puppy–An open-source software application and portable system design for low-cost manual measurements of CO_2 and H_2O fluxes. *Agricultural and Forest Meteorology* **274**: 1–6.

Chapin FS III, Schulze ED, Mooney HA. 1990. The ecology and economics of storage in plants. *Annual Review of Ecology and Systematics* **21**: 423–447.

D'Andrea E, Rezaie N, Battistelli A, Gavrichkova O, Kuhlmann I, Matteucci G, Moscatello S, Proietti S, Scartazza A, Trumbore S. 2019. Winter's bite: beech trees survive complete defoliation due to spring late-frost damage by mobilizing old C reserves. *New Phytologist* **224**: 625–631.

Dickman LT, McDowell NG, Sevanto S, Pangle RE, Pockman WT. 2015. Carbohydrate dynamics and mortality in a piñon-juniper woodland under three future precipitation scenarios. *Plant, Cell & Environment* **38**: 729–739.

Dietze MC, Sala A, Carbone MS, Czimczik CI, Mantooth JA, Richardson AD, Vargas R. 2014. Nonstructural carbon in woody plants. *Annual Review of Plant Biology* **65**: 667–687.

Epron D, Dreyer E, Bréda N. 1992. Photosynthesis of oak trees [*Quercus petraea* (Matt.) Liebl.] during drought under field conditions: diurnal course of net CO_2 assimilation and photochemical efficiency of photosystem II. *Plant, Cell & Environment* **15**: 809–820.

Fatichi S, Leuzinger S, Körner C. 2014. Moving beyond photosynthesis: from carbon source to sink-driven vegetation modeling. *New Phytologist* **201**: 1086–1095.

Fritts HC, Swetnam TW. 1989. Dendroecology: a tool for evaluating. *Advances in Ecological Research* **19**: 111–188.

Furze ME, Huggett BA, Aubrecht DM, Stolz CD, Carbone MS, Richardson AD. 2019. Whole-tree nonstructural carbohydrate storage and seasonal dynamics in five temperate species. *New Phytologist* **221**: 1466–1477.

Gamon JA, Pearcy RW. 1989. Leaf movement, stress avoidance and photosynthesis in *Vitis californica*. *Oecologia* **79**: 475–481.

Grossiord C, Sevanto S, Adams HD, Collins AD, Dickman LT, McBranch N, Michaletz ST, Stockton EA, Vigil M, McDowell NG. 2017. Precipitation, not air temperature, drives functional responses of trees in semi-arid ecosystems. *Journal of Ecology* **105**: 163–175.

Guo JS, Gear L, Hultine KR, Koch GW, Ogle K. 2020. Non-structural carbohydrate dynamics associated with antecedent stem water potential and air temperature in a dominant desert shrub. *Plant, Cell & Environment* **43**: 1467–1483.

Hagedorn F, Joseph J, Peter M, Luster J, Pritsch K, Geppert U, Kerner R, Molinier V, Egli S, Schaub M *et al.* 2016. Recovery of trees from drought depends on belowground sink control. *Nature Plants* **2**: 16111.

Hardie SML, Garnett MH, Fallick AE, Rowland AP, Ostle NJ. 2005. Carbon dioxide capture using a zeolite molecular sieve sampling system for isotopic studies (^{13}C and ^{14}C) of respiration. *Radiocarbon* **47**: 441–451.

He W, Liu H, Qi Y, Liu F, Zhu X. 2020. Patterns in nonstructural carbohydrate contents at the tree organ level in response to drought duration. *Global Change Biology* **26**: 3627–3638.

Herrera-Ramírez D, Muhr J, Hartmann H, Römermann C, Trumbore S, Sierra CA. 2020. Probability distributions of nonstructural carbon ages and transit times provide insights into carbon allocation dynamics of mature trees. *New Phytologist* **226**: 1299–1311.

Hilman B, Muhr J, Helm J, Kuhlmann I, Schulze E-D, Trumbore S. 2021. The size and the age of the metabolically active carbon in tree roots. *Plant, Cell & Environment* **44**: 2522–2535.

Hoch G, Richter A, Körner C. 2003. Non-structural carbon compounds in temperate forest trees. *Plant, Cell & Environment* **26**: 1067–1081.

Hsiao TC. 1973. Plant responses to water stress. *Annual Review of Plant Physiology* **24**: 519–570.

Hua Q, Turnbull JC, Santos GM, Rakowski AZ, Ancapichún S, De Pol-Holz R, Hammer S, Lehman SJ, Levin I, Miller JB. 2022. Atmospheric radiocarbon for the period 1950–2019. *Radiocarbon* **64**: 723–745.

Huang J, Hammerbacher A, Gershenzon J, van Dam NM, Sala A, McDowell NG, Chowdhury S, Gleixner G, Trumbore S, Hartmann H. 2021. Storage of carbon reserves in spruce trees is prioritized over growth in the face of carbon limitation. *Proceedings of the National Academy of Sciences, USA* **118**: e2023297118.

Hudson PJ, Limousin JM, Krofcheck DJ, Boutz AL, Pangle RE, Gehres N, McDowell NG, Pockman WT. 2018. Impacts of long-term precipitation manipulation on hydraulic architecture and xylem anatomy of piñon and juniper in Southwest USA. *Plant, Cell & Environment* **41**: 421–435.

Kannenberg SA, Schwalm CR, Anderegg WRL. 2020. Ghosts of the past: how drought legacy effects shape forest functioning and carbon cycling. *Ecology Letters* **23**: 891–901.

Katabuchi M. 2015. LEAFAREA: an R package for rapid digital image analysis of leaf area. *Ecological Research* **30**: 1073–1077.

Klein T, Hoch G, Yakir D, Körner C. 2014. Drought stress, growth and nonstructural carbohydrate dynamics of pine trees in a semi-arid forest. *Tree Physiology* **34**: 981–992.

Kolus HR, Huntzinger DN, Schwalm CR, Fisher JB, McKay N, Fang Y, Michalak AM, Schaefer K, Wei Y, Poulter B. 2019. Land carbon models underestimate the severity and duration of drought's impact on plant productivity. *Scientific Reports* **9**: 2758.

Kozlowski TT. 1992. Carbohydrate sources and sinks in woody plants. *The Botanical Review* **58**: 107–222.

Kunert N, Hajek P, Hietz P, Morris H, Rosner S, Tholen D. 2021. Summer temperatures reach the thermal tolerance threshold of photosynthetic decline in temperate conifers. *Plant Biology* **24**: 1254–1261.

Lacointe A, Kajji A, Daudet F-A, Archer P, Frossard J-S, Saint-Joanis B, Vandame M. 1993. Mobilization of carbon reserves in young walnut trees. *Acta Botanica Gallica* **140**: 435–441.

Landhäusser SM, Chow PS, Dickman LT, Furze ME, Kuhlman I, Schmid S, Wiesenbauer J, Wild B, Gleixner G, Hartmann H. 2018. Standardized protocols and procedures can precisely and accurately quantify non-structural carbohydrates. *Tree Physiology* **38**: 1764–1778.

Li W, Hartmann H, Adams HD, Zhang H, Jin C, Zhao C, Guan D, Wang A, Yuan F, Wu J. 2018. The sweet side of global change–dynamic responses of non-structural carbohydrates to drought, elevated CO_2 and nitrogen fertilization in tree species. *Tree Physiology* **38**: 1706–1723.

Lowe DC. 1984. Preparation of graphite targets for radiocarbon dating by tandem accelarator mass spectrometer (TAMS). *The International Journal of Applied Radiation and Isotopes* **35**: 349–352.

Mackay DS, Savoy PR, Grossiord C, Tai X, Pleban JR, Wang DR, McDowell NG, Adams HD, Sperry JS. 2020. Conifers depend on established roots during drought: results from a coupled model of carbon allocation and hydraulics. *New Phytologist* **225**: 679–692.

Maxwell K, Johnson GN. 2000. Chlorophyll fluorescence–a practical guide. *Journal of Experimental Botany* **51**: 659–668.

McDowell NG. 2011. Mechanisms linking drought, hydraulics, carbon metabolism, and vegetation mortality. *Plant Physiology* **155**: 1051–1059.

McDowell NG, Grossiord C, Adams HD, Pinzón-Navarro S, Mackay DS, Breshears DD, Allen CD, Borrego I, Dickman LT, Collins A. 2019. Mechanisms of a coniferous woodland persistence under drought and heat. *Environmental Research Letters* **14**: 45014.

McDowell NG, Sapes G, Pivovaroff A, Adams HD, Allen CD, Anderegg WRL, Arend M, Breshears DD, Brodribb T, Choat B *et al.* 2022. Mechanisms of woody plant mortality under rising drought, CO_2, and vapor pressure deficit. *Nature Reviews Earth and Environment* **3**: 294–308.

McDowell NG, Williams AP, Xu C, Pockman WT, Dickman LT, Sevanto S, Pangle R, Limousin J, Plaut J, Mackay DS *et al.* 2016. Multi-scale predictions of massive conifer mortality due to chronic temperature rise. *Nature Climate Change* **6**: 295–300.

Metzler H, Müller M, Sierra CA. 2018. Transit-time and age distributions for nonlinear time-dependent compartmental systems. *Proceedings of the National Academy of Sciences, USA* **115**: 1150–1155.

Monson RK, Trowbridge AM, Lindroth RL, Lerdau MT. 2022. Coordinated resource allocation to plant growth–defense tradeoffs. *New Phytologist* **233**: 1051–1066.

Muhr J, Trumbore S, Higuchi N, Kunert N. 2018. Living on borrowed time–Amazonian trees use decade-old storage carbon to survive for months after complete stem girdling. *New Phytologist* **220**: 111–120.

Muller B, Pantin F, Génard M, Turc O, Freixes S, Piques M, Gibon Y. 2011. Water deficits uncouple growth from photosynthesis, increase C content, and modify the relationships between C and growth in sink organs. *Journal of Experimental Botany* **62**: 1715–1729.

Pangle RE, Hill JP, Plaut JA, Yepez EA, Elliot JR, Gehres N, McDowell NG, Pockman WT. 2012. Methodology and performance of a rainfall manipulation experiment in a piñon–juniper woodland. *Ecosphere* **3**: 1–20.

Peltier D, Guo J, Nguyen P, Bangs M, Gear L, Wilson M, Jefferys S, Samuels-Crow K, Yocom LL, Liu Y. 2020. Temporal controls on crown nonstructural carbohydrates in southwestern US tree species. *Tree Physiology* **41**: 388–402.

Peltier D, LeMoine J, Ebert C, Xu X, Ogle K, Richardson A, Carbone M. 2023. An incubation method to determine the age of available nonstructural carbon in woody plant tissues. *Tree Physiology*: tpad015.

Peltier DM, Ogle K. 2020. Tree growth sensitivity to climate is temporally variable. *Ecology Letters* **23**: 1561–1572.

Peltier DMP, Fell M, Ogle K. 2016. Legacy effects of drought in the southwestern United States: a multi-species synthesis. *Ecological Monographs* **86**: 312–326.

Peltier DMP, Ogle K. 2019. Legacies of more frequent drought in ponderosa pine across the western United States. *Global Change Biology* **25**: 3803–3816.

Plaut JA, Wadsworth WD, Pangle R, Yepez EA, McDowell NG, Pockman WT. 2013. Reduced transpiration response to precipitation pulses precedes mortality in a piñon-juniper woodland subject to prolonged drought. *New Phytologist* **200**: 375–387.

Plaut JA, Yepez EA, Hill J, Pangle R, Sperry JS, Pockman WT, Mcdowell NG. 2012. Hydraulic limits preceding mortality in a piñon–juniper woodland under experimental drought. *Plant, Cell & Environment* **35**: 1601–1617.

R Core Team. 2022. *R: a language and environment for statistical computing.* Vienna, Austria: R Foundation for Statistical Computing.

Rehschuh R, Cecilia A, Zuber M, Faragó T, Baumbach T, Hartmann H, Jansen S, Mayr S, Ruehr N. 2020. Drought-induced xylem embolism limits the recovery of keaf gas exchange in Scots pine. *Plant Physiology* **184**: 852–864.

Resco de Dios V, Gessler A. 2021. Sink and source co-limitation in the response of stored non-structural carbohydrates to an intense but short drought. *Trees* **36**: 1–4.

Richardson AD, Carbone MS, Huggett BA, Furze ME, Czimczik CI, Walker JC, Xu X, Schaberg PG, Murakami P. 2015. Distribution and mixing of old and new nonstructural carbon in two temperate trees. *New Phytologist* **206**: 590–597.

Richardson AD, Carbone MS, Keenan TF, Czimczik CI, Hollinger DY, Murakami P, Schaberg PG, Xu X. 2013. Seasonal dynamics and age of stemwood nonstructural carbohydrates in temperate forest trees. *New Phytologist* **197**: 850–861.

Rood SB, Patiño S, Coombs K, Tyree MT. 2000. Branch sacrifice: cavitation-associated drought adaptation of riparian cottonwoods. *Trees* **14**: 248–257.

Rowland L, da Costa AC, Oliveira RS, Bittencourt PR, Giles AL, Coughlin I, de Britto CP, Bartholomew D, Domingues TF, Miatto RC. 2021. The response of carbon assimilation and storage to long-term drought in tropical trees is dependent on light availability. *Functional Ecology* **35**: 43–53.

Schwalm CR, Anderegg WR, Michalak AM, Fisher JB, Biondi F, Koch G, Litvak M, Ogle K, Shaw JD, Wolf A *et al.* 2017. Global patterns of drought recovery. *Nature* **548**: 202–205.

Sevanto S, McDowell NG, Dickman LT, Pangle R, Pockman WT. 2014. How do trees die? A test of the hydraulic failure and carbon starvation hypotheses. *Plant, Cell & Environment* **37**: 153–161.

Sierra CA, Müller M, Trumbore SE. 2012. Models of soil organic matter decomposition: the SOILR package, v.1.0. *Geoscientific Model Development* **5**: 1045–1060.

Smith AM, Stitt M. 2007. Coordination of carbon supply and plant growth. *Plant, Cell & Environment* **30**: 1126–1149.

Spicer R. 2005. Senescence in secondary xylem: heartwood formation as an active developmental program. In: Holbrook NM, Zwieniecki MA, eds. *Vascular transport in plants.* Cambridge, MA, USA: Academic Press, 457–475.

Synal H-A, Stocker M, Suter M. 2007. MICADAS: a new compact radiocarbon AMS system. *Nuclear Instruments and Methods in Physics Research Section B: Beam Interactions with Materials and Atoms* **259**: 7–13.

Thompson RA, Adams HD, Breshears DD, Collins AD, Dickman LT, Grossiord C, Manrique-Alba À, Peltier DM, Ryan MG, Trowbridge AM. 2023. No carbon storage in growth-limited trees in a semi-arid woodland. *Nature Communications* **14**: 1959.

Trowbridge AM, Adams HD, Collins A, Dickman LT, Grossiord C, Hofland M, Malone S, Weaver DK, Sevanto S, Stoy PC. 2021. Hotter droughts alter resource allocation to chemical defenses in piñon pine. *Oecologia* **197**: 921–938.

Trugman AT, Detto M, Bartlett MK, Medvigy D, Anderegg WRL, Schwalm C, Schaffer B, Pacala SW. 2018. Tree carbon allocation explains forest drought-kill and recovery patterns. *Ecology Letters* **21**: 1552–1560.

Trumbore SE, Sierra CA, Hick Pries C. 2016. Radiocarbon nomenclature, theory, models, and interpretation: measuring age, determining cycling rates, and tracing source pools. In: Schuur EAG, Druffel ERM, Trumbore SE, eds. *Radiocarbon and climate change*. Cham, Switzerland: Springer International Publishing, 45–82.

Tsamir-Rimon M, Ben-Dor S, Feldmesser E, Oppenhimer-Shaanan Y, David-Schwartz R, Samach A, Klein T. 2021. Rapid starch degradation in the wood of olive trees under heat and drought is permitted by three stress-specific beta amylases. *New Phytologist* **229**: 1398–1414.

Vargas R, Trumbore SE, Allen MF. 2009. Evidence of old carbon used to grow new fine roots in a tropical forest. *New Phytologist* **182**: 710–718.

Vogel JS, Southon JR, Nelson DE, Brown TA. 1984. Performance of catalytically condensed carbon for use in accelerator mass spectrometry. *Nuclear Instruments and Methods in Physics Research Section B: Beam Interactions with Materials and Atoms* **5**: 289–293.

Wang W, English NB, Grossiord C, Gessler A, Das AJ, Stephenson NL, Baisan CH, Allen CD, McDowell NG. 2020. Mortality predispositions of conifers across western USA. *New Phytologist* **229**: 831–844.

Wiley E, Rogers BJ, Hodgkinson R, Landhäusser SM. 2016. Nonstructural carbohydrate dynamics of lodgepole pine dying from mountain pine beetle attack. *New Phytologist* **209**: 550–562.

Williams AP, Cook BI, Smerdon JE. 2022. Rapid intensification of the emerging southwestern North American megadrought in 2020–2021. *Nature Climate Change* **12**: 232–234.

Williams AP, Cook ER, Smerdon JE, Cook BI, Abatzoglou JT, Bolles K, Baek SH, Badger AM, Livneh B. 2020. Large contribution from anthropogenic warming to an emerging North American megadrought. *Science* **368**: 314–318.

Zhang P, Jeong J-H, Yoon J-H, Kim H, Wang S-YS, Linderholm HW, Fang K, Wu X, Chen D. 2020. Abrupt shift to hotter and drier climate over inner East Asia beyond the tipping point. *Science* **370**: 1095–1099.

Supporting Information

Additional Supporting Information may be found online in the Supporting Information section at the end of the article.

Fig. S1 Site meteorological data.

Fig. S2 Bole chamber information.

Fig. S3 Atmospheric radiocarbon for the period 1950–2019 and annual samples.

Fig. S4 Plot soil temperature and volumetric water content.

Fig. S5 Needle, twig, and root non-structural carbohydrates concentrations.

Fig. S6 Tree-ring time-series.

Fig. S7 $\Delta^{14}C$ relationships with other covariates.

Fig. S8 Leaf stomatal conductance data.

Methods S1 JAGS code to specify Bayesian models used in data analysis.

Methods S2 Forward simulation of heterogeneous tree reserve non-structural carbohydrates pools.

Table S1 Full accelerator mass spectrometry dataset.

Please note: Wiley is not responsible for the content or functionality of any Supporting Information supplied by the authors. Any queries (other than missing material) should be directed to the *New Phytologist* Central Office.